Regulation by a chaperone improves substrate selectivity during cotranslational protein targeting

Aileen Ariosa[1], Jae Ho Lee, Shuai Wang, Ishu Saraogi[2], and Shu-ou Shan[3]

Division of Chemistry and Chemical Engineering, California Institute of Technology, Pasadena, CA 91125

Edited by Jonathan S. Weissman, University of California, San Francisco, Howard Hughes Medical Institute, and California Institute for Quantitative Biosciences, San Francisco, CA, and approved May 5, 2015 (received for review November 25, 2014)

The ribosome exit site is a crowded environment where numerous factors contact nascent polypeptides to influence their folding, localization, and quality control. Timely and accurate selection of nascent polypeptides into the correct pathway is essential for proper protein biogenesis. To understand how this is accomplished, we probe the mechanism by which nascent polypeptides are accurately sorted between the major cotranslational chaperone trigger factor (TF) and the essential cotranslational targeting machinery, signal recognition particle (SRP). We show that TF regulates SRP function at three distinct stages, including binding of the translating ribosome, membrane targeting via recruitment of the SRP receptor, and rejection of ribosome-bound nascent polypeptides beyond a critical length. Together, these mechanisms enhance the specificity of substrate selection into both pathways. Our results reveal a multilayered mechanism of molecular interplay at the ribosome exit site, and provide a conceptual framework to understand how proteins are selected among distinct biogenesis machineries in this crowded environment.

signal recognition particle | trigger factor | ribosome | protein biogenesis | GTPases

Proper protein biogenesis is a prerequisite for the maintenance of a functional proteome. Accumulating data indicate that this process begins at the ribosome exit site, where many protein biogenesis machineries can interact and gain access to the nascent polypeptide. This includes chaperones (1–5) such as trigger factor (TF) (1, 4, 6, 7), Hsp70, and the nascent polypeptide-associated complex (8–13); modification enzymes (10, 14–16) such as *N*-acetyl transferase, methionine aminopeptidase, and arginyl transferase; protein-targeting and translocation machineries such as signal recognition particle (SRP) (17–20), SecA (21), the SecYEG (or Sec61p) (22, 23) and YidC translocases (24, 25), and the ribosome-bound quality control complex (26–30). Engagement of these factors with nascent polypeptides influences their folding, assembly, localization, processing, and quality control. Within seconds after the nascent polypeptide emerges from the ribosomal exit tunnel, it must engage the correct set of factors and thus commit to the proper biogenesis pathway. How this is accomplished in the crowded environment at the ribosome exit site is an emerging question. In this work, we address this question by deciphering how nascent proteins are selected between two major protein biogenesis machineries in bacteria, SRP and TF.

SRP is a universally conserved ribonucleoprotein complex responsible for the cotranslational targeting of proteins to the eukaryotic endoplasmic reticulum (ER), or the bacterial plasma membrane (31). SRP recognizes ribosome-nascent chain complexes (termed RNC or cargo) carrying strong signal sequences and delivers them to the SecYEG or YidC translocation machinery on the target membrane. SRP binds RNC via two interactions: a helical N domain in the SRP54 protein (called Ffh in bacteria) binds the ribosomal protein L23, and a methionine-rich M domain binds hydrophobic signal sequences on nascent proteins as they emerge from the translating ribosome (Fig. 1*A*). Both SRP and SRP receptor (called FtsY in bacteria) also contain a conserved NG domain, comprised of a GTPase (guanosine 5′-triphosphate hydrolase) G domain and the N domain, whose direct interaction mediates the delivery of cargo to the target membrane.

Biophysical analyses (32–34) showed that membrane targeting is a two-step process in which SRP and FtsY first associate via their N domains to form a transient early intermediate (31, 32, 35). GTP (guanosine 5′-triphosphate)-driven rearrangements then bring the G domains of both proteins into close contact, giving a stable closed complex (36, 37). This rearrangement also exposes a membrane-binding helix of FtsY and thus is coupled to the membrane targeting of cargo (38). Importantly, SRP•FtsY assembly contributes extensively to the fidelity of SRP (39). The initial recognition of RNC by SRP is insufficient to reject suboptimal cargos bearing weak signal sequences (40, 41). Instead, a correct cargo strongly stabilizes the otherwise labile *early* intermediate and thus accelerates formation of the SRP•FtsY closed complex over 10^3-fold, whereas suboptimal cargos provide much less stimulation (34, 40, 42). This enables rapid delivery of the correct cargos to the target membrane and provides kinetic discrimination against suboptimal cargos (Fig. S1).

TF is a major cotranslational chaperone in bacteria, with an estimated cellular concentration of 50–80 μM (6). With a dissociation constant (K_d) of ∼1 μM for ribosomes (43), TF is bound to virtually every ribosome in the cell. Like SRP, TF contacts the ribosome via the L23 and L29 proteins near the

Significance

Correct protein biogenesis is crucial for all cells. Numerous factors including molecular chaperones, modification enzymes, and protein-targeting machineries bind near the ribosome exit site and can access the nascent protein. How nascent proteins are accurately selected into the correct biogenesis pathway in such a crowded environment is an emerging question central to accurate protein biogenesis. Using chemical biology and biochemical and biophysical tools, we show that the major cotranslational chaperone, trigger factor, and cotranslational targeting machinery, signal recognition particle, regulate each other at multiple stages, including initial binding, ribosome delivery to the membrane, and enforcement of a timer for cotranslational protein targeting. Together, these mechanisms enhance accurate substrate selection into both cotranslational and posttranslational protein targeting pathways.

Author contributions: A.A., J.H.L., and S.-o.S. designed research; A.A., J.H.L., S.W., I.S., and S.-o.S. performed research; A.A., J.H.L., S.W., I.S., and S.-o.S. analyzed data; and A.A. and S.-o.S. wrote the paper.

The authors declare no conflict of interest.

This article is a PNAS Direct Submission.

[1]Present address: Life Sciences Institute, University of Michigan, Ann Arbor, MI 48109.

[2]Present address: Department of Chemistry, Indian Institute of Science Education and Research, Bhopal, MP 462 066, India.

[3]To whom correspondence should be addressed. Email: sshan@caltech.edu.

This article contains supporting information online at www.pnas.org/lookup/suppl/doi:10.1073/pnas.1422594112/-/DCSupplemental.

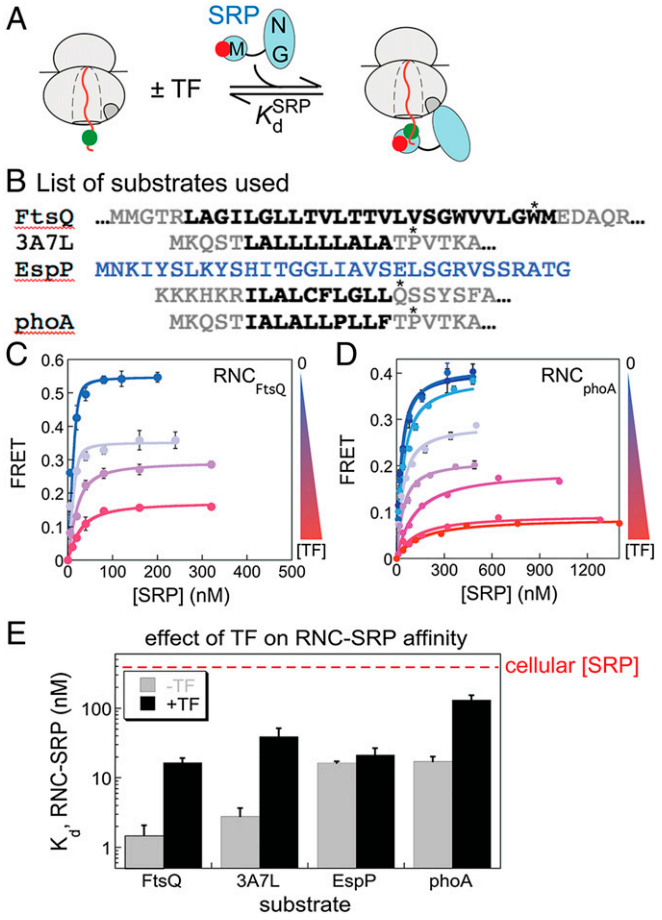

Fig. 1. TF binds to SRP-occupied RNCs and weakens SRP binding. (*A*) Schematic depiction of the FRET assay to measure RNC–SRP binding. Green dot denotes Cm (donor); red dot denotes BODIPY FL (acceptor). (*B*) N-terminal sequences of the different substrates used in this study. Bold highlights the hydrophobic core of the signal sequences. Asterisk denotes the position where the amino acid is replaced by the Cm dye. (*C* and *D*) Equilibrium titrations for RNC–SRP binding in the presence of increasing TF concentration (indicated as increasing shades of red). The data were fitted to Eq. **S2** and yielded the following parameters. (*C*) Apparent K_d values for RNC$_{FtsQ}$ binding of 1.1 nM, 1.5 nM, 9.2 nM, and 16.6 nM and FRET end points of 0.54, 0.35, 0.29, and 0.17, respectively, with 0 μM, 1 μM, 5 μM, and 30 μM TF present. (*D*) Apparent K_d values for RNC$_{phoA}$ binding of 17.2 nM, 21.1 nM, 30.3 nM, 28.3 nM, 31.5 nM, 104.5 nM, 106.3 nM, and 131.9 nM and FRET end points of 0.40, 0.41, 0.39, 0.29, 0.21, 0.19, 0.09, and 0.08, respectively, with 0 μM, 0.1 μM, 0.2 μM, 0.5 μM, 1 μM, 2 μM, 5 μM, and 10 μM TF present. (*E*) Summary of the effect of TF on apparent RNC–SRP binding affinity with the different substrates. The red dashed line denotes the cellular SRP concentration. Error bars are shown but may not be visible. Error bars are SDs from two to three measurements.

ribosome exit site (3, 5, 44). Also analogous to SRP, TF preferentially interacts with hydrophobic sequences on the nascent polypeptide (1, 2, 4, 45, 46), mediated by a large concave surface rich in hydrophobic residues (1, 3–6). Despite these similarities with SRP, TF directs substrate proteins to distinct biogenesis pathways: It exhibits synthetic lethality with DnaK/J and facilitates the productive folding of cytosolic proteins (1, 4, 7, 9, 11). It also interacts with a subset of secretory and outer membrane proteins and interfaces with the posttranslational SecA/B pathway (8, 10, 12–14).

SRP and TF are two distinct biogenesis pathways that a nascent protein must commit to. This raises intriguing questions: How do these two factors, which have overlapping substrate preferences, compete and/or collaborate at the ribosome exit site? How are nascent proteins sorted between them and committed to the correct pathway in a timely and accurate manner? Extensive past work to address these questions has led to different (and sometimes contradictory) models, including (*i*) TF and SRP compete for binding to the RNC (10, 15, 16, 18); (*ii*) TF and SRP can bind to the same RNC simultaneously (17, 19–21); (*iii*) FtsY rejects TF from SRP-bound ribosomes (17); and (*iv*) TF preferentially occupies longer nascent chains (13, 45–47) and, by inference, SRP preferentially binds short nascent chains. A unifying model that reconciles all these observations and explains how nascent chains on the ribosome are selected by TF or SRP is still lacking. Most importantly, most of the previous studies have focused on the initial binding of SRP or TF to the nascent polypeptide, which may not be the step at which nascent proteins are committed to their respective biogenesis pathways.

In this work, we used high-resolution biochemical and biophysical analyses to investigate the interplay between TF and SRP at the ribosome exit site in molecular detail. We show that TF regulates SRP function by three distinct mechanisms, which together enhance the ability of the SRP pathway to reject suboptimal substrates. Our results establish a comprehensive and cohesive model that explains previous observations, delineates the complex interplay between protein biogenesis factors at the ribosome exit site, and provides a conceptual foundation to understand how timely and accurate selection of substrates is achieved in this crowded environment.

Results

Anticooperative Binding of SRP and TF to RNC. We first asked how TF affects cargo recognition by SRP as the nascent polypeptide emerges from the ribosome exit tunnel. To this end, we used amber suppression technology to incorporate a fluorescent nonnatural amino acid, 7-hydroxycoumaryl ethylglycine (Cm), into the nascent polypeptide downstream of the signal sequence (Fig. 1 *A* and *B*, asterisks) (48). When paired with SRP labeled with BODIPY FL at residue 421 in the Ffh M domain, efficient Förster resonance energy transfer (FRET) was observed (48), providing a highly specific and sensitive assay to report on the interaction of SRP with nascent polypeptides on RNC.

To test whether TF helps enhance the specificity of SRP, we used a range of substrates with varying dependence on SRP (Fig. 1*B*). FtsQ, a bona fide SRP substrate, uses an integral transmembrane domain (TMD) as the signal sequence (18, 49). An engineered substrate, 3A7L, contains a modestly hydrophobic signal sequence more representative of SRP-dependent secretory proteins. (40). As suboptimal substrates, we used EspP, a SecA/B substrate that is rejected by SRP due to its N-terminal extension (40, 50, 51), and phoA, a primarily SecA-dependent substrate whose signal sequence is less hydrophobic (52, 53). For all of the experiments in Figs. 1–4, we purified homogeneous stalled RNCs with 80–85 amino acids between the start of signal sequence and the peptidyl transferase center of ribosome. This mimics the stage at which the signal sequence emerges from the ribosome exit tunnel and is optimal for recognition by SRP (47, 54).

There has been extensive debate on whether TF and SRP compete with one another for binding RNCs (Fig. S2*A*), or whether they bind the same RNC (Fig. S2*B*) (10, 15–17, 19, 20). Well-established theoretical treatments (55) and kinetic simulations (Fig. S2*B*) show that these alternative models can be rigorously distinguished by quantitatively analyzing the effect of TF on SRP–RNC binding using our conformation-sensitive FRET assay. If binding of TF and SRP to RNCs is mutually exclusive, then TF will deplete the free RNCs available to bind SRP, necessitating higher SRP concentrations to reach saturation (Fig. S2*A*). Further, when SRP is allowed to bind RNC at saturating concentrations, TF cannot alter the conformation and, hence, the FRET value of the RNC•SRP complex (Fig. S2*A*).

In contrast, if TF alters the FRET value of the RNC•SRP complex, then this rules out a strictly competitive model and could only be explained by a model in which TF and SRP bind to the same RNC and alter each other's interaction with the nascent polypeptide (Fig. S2*B*). TF could either strengthen (cooperative) or weaken (anticooperative) SRP binding to the RNC; the latter model is simulated in Fig. S2*B*.

A recent study measured how SRP (or TF) altered RNC binding to TF (or SRP) using FRET between ribosomal protein L23 and TF (or SRP). Nevertheless, a cobinding model was assumed, rather than tested, in this analysis (20). Indeed, the low signal-to-noise ratio of this assay (often 10–20%) led to ambiguous interpretations: Although some data appeared consistent with a competitive model (Fig. S2*A*), others appeared consistent with a cobinding model (Fig. S2*B*) (20). The robust FRET between SRP (or TF) and signal sequence allowed us to more unambiguously test and distinguish between these models. Equilibrium titrations of RNC–SRP binding showed that, with all four substrates, increasing amounts of TF induced two significant changes: (*i*) Increasingly higher SRP concentrations are required to reach saturation, and (*ii*) there are successive reductions in FRET efficiency when the RNC•SRP complex is formed at saturating concentrations (Fig. 1 *C* and *D* and Fig. S2 *C* and *D*). These results provide strong evidence for anticooperative binding of TF and SRP to the RNC, but are incompatible with models in which their binding to RNC is mutually exclusive (Fig. S2*A*). In addition, the effect of TF on the observed RNC–SRP binding affinity (app K_d^{SRP}) is saturable (Fig. S2*E*). This is also consistent with predictions from the model in which TF and SRP bind to the same RNC, but is incompatible with models in which their binding is mutually exclusive (Fig. S2*F*).

If TF weakens the affinity of SRP for RNC, then reciprocally, SRP would weaken the affinity of TF for RNC. To test this prediction, we developed a FRET assay to measure RNC–TF interaction. We labeled TF with BODIPY FL at an engineered cysteine (C377) which, when paired with Cm-labeled RNC, induced efficient FRET (Fig. 2 *A* and *B*). Equilibrium titrations using this FRET assay showed that TF binds tightly to all of the RNCs tested, with K_d^{TF} values ranging from 2.5 nM to 8.4 nM (Fig. 2 *C* and *D* and Fig. S3 *A* and *B*, blue lines; Fig. 2*E*, gray bars). As expected, replacement of residues F44, R45, and K46 with alanine (FRK→AAA mutant), which was reported to weaken TF interaction with the ribosome (44), weakened TF–RNC binding affinity threefold to fourfold (Fig. S3*A*). Addition of SRP induced two changes in RNC–TF binding: (*i*) a modest weakening of the binding affinity between TF and RNC and (*ii*) an altered FRET efficiency when the RNC•TF complex is formed at saturating TF concentrations (Fig. 2 *C* and *D* and Fig. S3 *B* and *C*). Further, the effect of SRP on the observed RNC–TF binding affinity (app K_d^{TF}) is saturable (Fig. S3*D*). This provides independent evidence for anticooperative binding between SRP and TF at the RNC (Fig. S2*B*).

Collectively, these results provide more conclusive evidence that TF and SRP can bind to the same RNC, on which they alter the binding affinities and conformation of one another (17, 19, 20). Importantly, these modulations did not lead to significant consequences on the occupancy of SRP or TF on the RNCs. As the cellular TF concentration (>50 μM) is over 10^3-fold higher than the weakest RNC–TF affinity observed here, the effect from SRP has negligible consequences on the occupancy of TF on the RNCs. Although SRP is less abundant (~400 nM), all of the RNC–SRP dissociation constants are still below the cellular SRP concentration in the presence of TF (Fig. 1*E*). A numerical analysis based on this information shows that TF would modestly influence SRP occupancy on RNC_{phoA} but not for the other RNCs tested (see more discussion in *TF Enhances the Specificity of SRP-Dependent Protein Targeting*). Further, binding of SRP to RNC_{EspP} is comparable to RNC_{FtsQ} or RNC_{3A7L} in the presence of TF

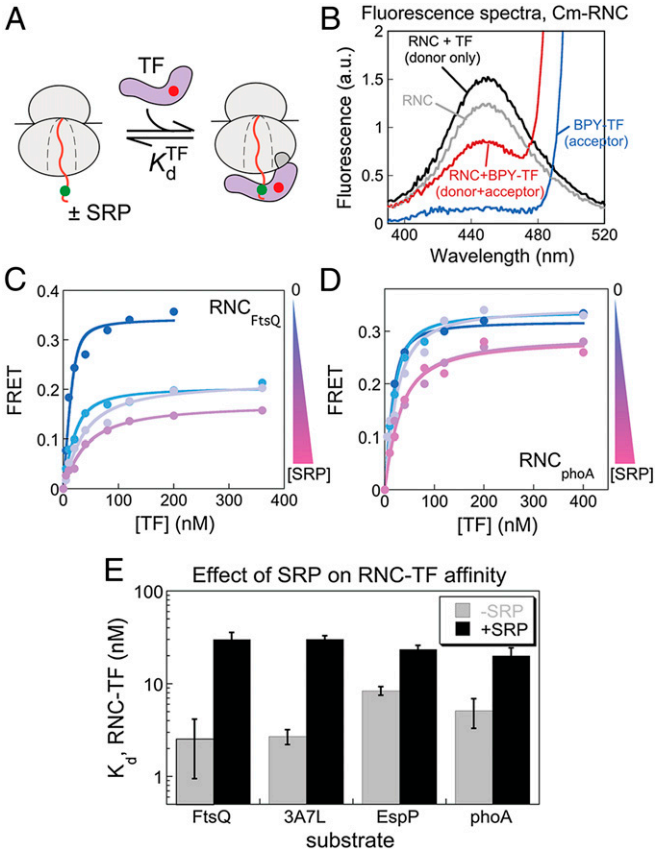

Fig. 2. SRP binds TF-occupied RNCs and weakens the binding of TF. (*A*) Scheme depicting the FRET assay to measure TF binding to RNC. Green dot denotes Cm (donor); red dot denotes BODIPY (acceptor). (*B*) Fluorescence emission spectra for Cm-labeled RNC (gray), BODIPY-labeled TF (BPY-TF, blue), and Cm-RNC in the presence of unlabeled TF (black) or BPY-TF (red). (*C* and *D*) Representative equilibrium titrations for RNC–TF binding in the presence of increasing SRP concentration (indicated as increasing shades of red). The data were fitted to Eq. **S2** and yielded the following parameters. (*C*) Apparent K_d values for TF–RNC_{FtsQ} binding of 2.6 nM, 9.2 nM, 26 nM, and 30 nM and FRET end points of 0.34, 0.21, 0.22, and 0.17, respectively, with 0 nM, 100 nM, 200 nM, and 400 nM SRP present. (*D*) Apparent K_d values for RNC_{phoA} binding of 5.1 nM, 7.6 nM, 13.1 nM, 20.9 nM, and 19.5 nM and FRET end points of 0.32, 0.33, 0.35, 0.29, and 0.29, respectively, with 0 nM, 100 nM, 200 nM, 400 nM, and 800 nM SRP present. (*E*) Summary of the effect of SRP on the apparent RNC–TF binding affinity for the different substrates. Error bars are SDs from two to three experiments.

(Fig. 1*E*). Therefore, at cellular concentrations, significant amounts of RNC•SRP•TF ternary complexes accumulate for both the SRP and SecA/B pathway substrates, and substrate commitment to SRP or TF does not primarily occur at the RNC-binding stage.

TF Slows the Recruitment of SRP Receptor to Suboptimal Cargos. We therefore examined the next step of the SRP pathway, cargo delivery to the target membrane mediated by SRP•FtsY assembly. Kinetic regulation of this process plays a key role in the ability of SRP to reject suboptimal substrates (34, 40). We asked whether TF increases substrate discrimination by SRP during this process.

Stable SRP•FtsY assembly is a two-step process in which a transient early intermediate is initially formed, followed by a GTP-dependent rearrangement to form a stable closed complex (32). The stability of the early intermediate directly correlates with the rate at which the closed complex is formed, and represents a major commitment step for correct cargos (33, 40, 41). We therefore tested how TF affects formation of the early targeting

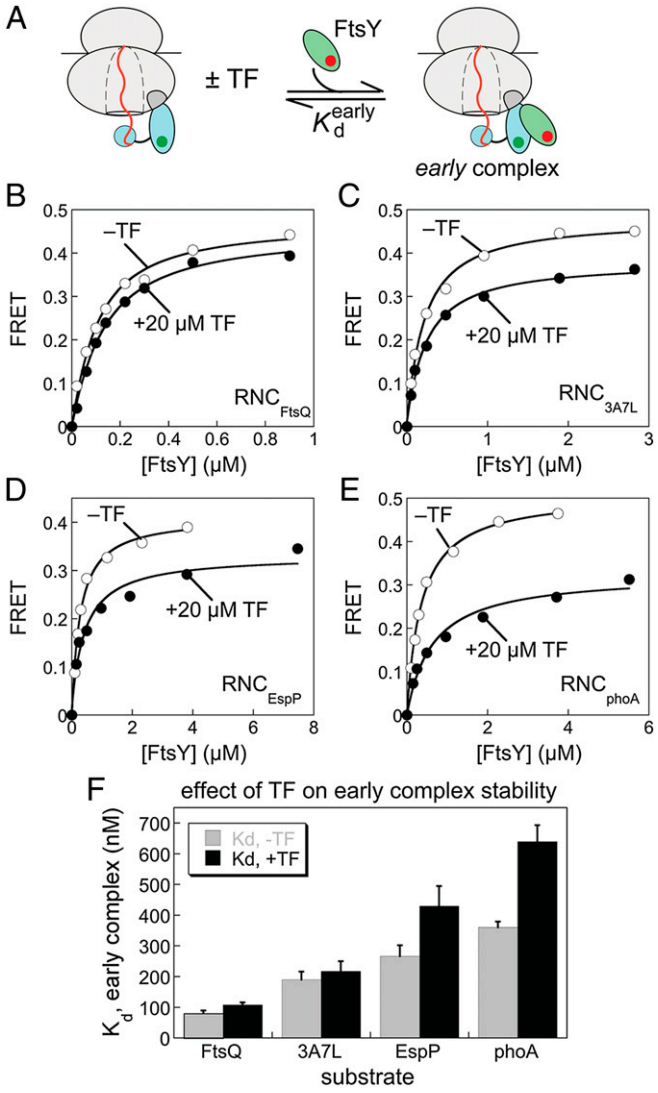

Fig. 3. TF induces formation of a weaker and distorted RNC•SRP•FtsY early complex. (*A*) Scheme depicting the FRET assay for measuring the formation of the *early* complex. (*B–E*) Representative equilibrium titrations for formation of the early targeting complex without (○) or with (●) 20 μM TF present for SRP loaded with 450 nM RNC_{FtsQ} (*B*), 400 nM RNC_{3A7L} (*C*), 600 nM RNC_{EspP} (*D*), and 1 μM RNC_{phoA} (*E*). The data were fitted to Eq. **S3** and yielded the following parameters: (*B*) K_d values of 80 nM and 108 nM and FRET end points of 0.47 and 0.45, respectively, with and without TF; (*C*) K_d values of 191 nM and 218 nM and FRET end points of 0.47 and 0.37, respectively, with and without TF; (*D*) K_d values of 266 nM and 428 nM and FRET end points of 0.42 and 0.32, respectively, with and without TF; and (*E*) K_d values of 358 nM and 640 nM and FRET end points of 0.51 and 0.33, respectively, with and without TF. (*F*) Summary of the effects of TF on the stability of the early complex formed with the different substrates. Error bars are SDs from 2 to 3 independent experiments.

complex. To this end, we assembled ternary RNC•SRP•TF complexes using saturating concentrations of the respective RNC and TF, as established by the results in Figs. 1 and 2 and Figs. S2 and S3. Because the early intermediate can form with or without GTP but its subsequent rearrangement is strictly GTP dependent, we isolated the early intermediate by leaving out GTP analogs during complex assembly with FtsY (32, 33, 56). Formation of the SRP•FtsY complex was monitored using FRET between *N*-(7-dimethylamino-4-methylcoumarin-3yl)-maleimide (DACM)-labeled at SRP C153 and BODIPY-labeled at FtsY C345 (Fig. 3*A*) (32, 33). Equilibrium titrations using this assay showed that, with a bona fide SRP substrate such as RNC_{FtsQ}, a highly stabilized SRP•FtsY early complex is formed, and TF has negligible effects on its stability or FRET efficiency (Fig. 3*B*). As the signal sequence becomes weaker, the RNC•SRP•FtsY early complex becomes less stable, as reported previously (40). Importantly, TF further weakens the early complex, and this effect is more substantial as the signal sequence becomes weaker (Fig. 3 *C–E*; summarized in Fig. 3*F*). Further, TF lowers the FRET efficiency when the early targeting complex is formed at saturating FtsY concentrations; this effect also becomes more pronounced as the signal sequence becomes weaker (Fig. 3 *B–E*). This indicates that TF alters the conformation of the SRP•FtsY early complexes formed with weaker SRP substrates, such that the G domains of SRP and FtsY (where the FRET probes are located) are positioned farther apart.

If TF induces the formation of a weaker and distorted early targeting complex for RNCs bearing weaker signal sequences, then assembly of the stable closed SRP•FtsY complex with these substrates will be significantly slowed by TF. To test this hypothesis, we compared the kinetics of SRP•FtsY closed complex assembly between preformed RNC•SRP and RNC•SRP•TF complexes. Complex assembly was measured using the same FRET assay but in the presence of GMPPNP (5′-guanylyl imidodiphosphate), which allows the early intermediate to proceed to the closed complex (Fig. 4*A*). Independent measurements using a fluorescent probe that specifically detects the closed complex have yielded rate constants comparable to the FRET assay (40). With strong SRP substrates such as FtsQ, complex formation is rapid and unaffected by TF (Fig. 4 *B* and *F*). With 3A7L, TF slows SRP•FtsY closed complex assembly threefold (Fig. 4 *C* and *F*). With SRP-independent substrates such as EspP and phoA, TF slows closed complex assembly more substantially, 10- to 12-fold (Fig. 4 *D* and *F*). Thus, although SRP can strongly discriminate between authentic and suboptimal cargos via the kinetics of FtsY recruitment, TF enhances this discrimination by an additional order of magnitude.

TF More Effectively Inhibits SRP as the Nascent Chain Elongates. It has been a long-standing observation that, as the nascent polypeptide elongates beyond a critical length of 130–140 amino acids, SRP loses its ability to target even the RNCs bearing SRP-dependent secretory proteins such as preprolactin (47, 57). This imposes a limited time window for SRP and FtsY to complete targeting, especially in bacteria where translation elongation occurs rapidly and SRP does not delay translation. However, the molecular basis underlying this phenomenon has been controversial. Some studies suggest that RNC–SRP binding affinity is reduced as the nascent chain becomes longer, whereas others suggest that SRP loses the ability to target longer nascent chains to the membrane (47, 57, 58).

To address this question, we prepared RNCs bearing longer nascent chains, with 130–135 amino acids from the N terminus of the signal sequence to the peptidyl transferase center. Using the FRET assays described above, we tested whether and how a longer nascent chain length affects cargo recognition by SRP (K_d^{SRP}) and assembly of the closed RNC•SRP•FtsY complex (k_{on}; Fig. 5*A*). Intriguingly, a longer nascent chain length exerted modest effects on RNC–SRP binding affinities (Table 1 and Fig. S4). Importantly, the SRP–$RNC_{130–135}$ binding affinities observed here (Table 1) and elsewhere (58) are still in the low nanomolar range and sufficient for SRP to occupy the RNC at its cellular concentration. Likewise, a longer nascent chain slows SRP•FtsY closed complex assembly by less than threefold (Table 2). These differences, although statistically significant and reproducible, are insufficient by themselves to lead to rejection of long-chain RNCs from the SRP pathway.

We asked whether TF could contribute to this rejection. We first tested how TF affects the binding of SRP to RNCs with longer nascent chains. Analogous to observations with shorter

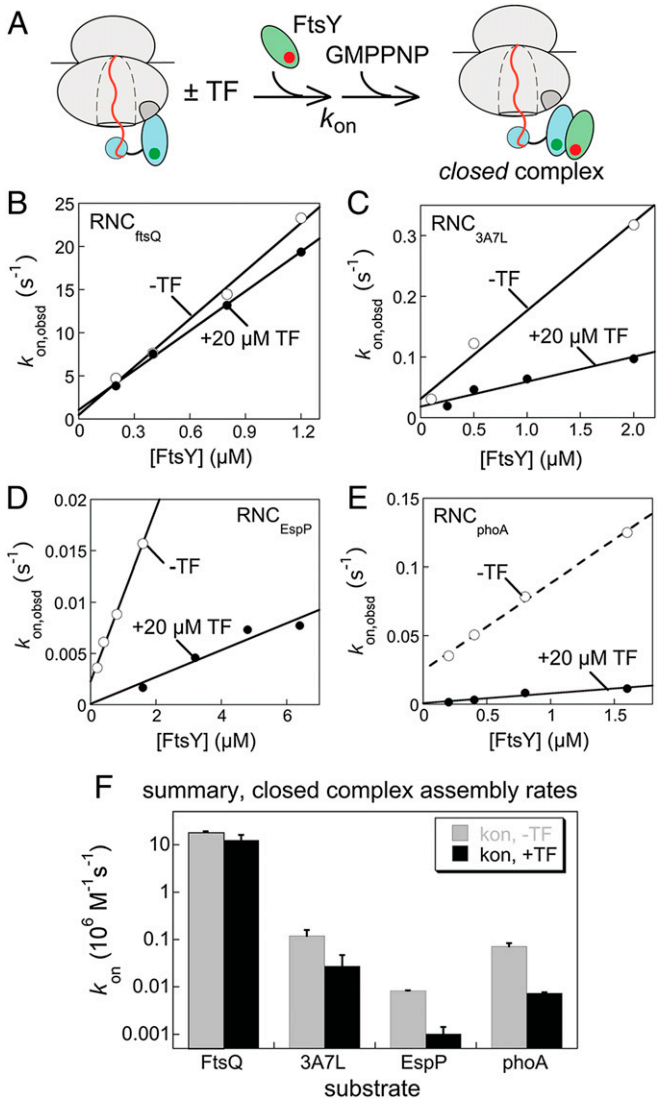

Fig. 4. TF selectively slows SRP•FtsY closed complex assembly with the suboptimal cargos. (*A*) Scheme for the FRET assay to measure the kinetics of SRP•FtsY closed complex assembly (k_{on}). (*B–E*) Representative measurements of association rate constants for SRP•FtsY closed complex assembly in the absence and presence of 20 μM TF, for SRP loaded with 800 nM RNC_{FtsQ} (*B*), 350 nM RNC_{3A7L} (*C*), 500 nM RNC_{EspP} (*D*), and 800 nM RNC_{phoA} (*E*). The data were fitted to Eq. **S4** and yielded the following values of k_{on}: (*B*) 18.5 × 10^6 $M^{-1}{\cdot}s^{-1}$ and 16.2 × 10^6 $M^{-1}{\cdot}s^{-1}$ with and without TF present, respectively; (*C*) 1.45 × 10^5 $M^{-1}{\cdot}s^{-1}$ and 0.41 × 10^5 $M^{-1}{\cdot}s^{-1}$ with and without TF present, respectively; (*D*) 8.4 × 10^3 $M^{-1}{\cdot}s^{-1}$ and 1.3 × 10^3 $M^{-1}{\cdot}s^{-1}$ with and without TF present, respectively; and (*E*) 6.3 × 10^4 $M^{-1}{\cdot}s^{-1}$ and 0.71 × 10^4 $M^{-1}{\cdot}s^{-1}$ with and without TF present, respectively. (*F*) Summary of the effect of TF on the rate of SRP•FtsY closed complex assembly with different substrates. Error bars are SDs from two to three independent experiments.

nascent chains, we observed anticooperative binding between TF and SRP to RNCs with a nascent chain length of 130–135 amino acids (Fig. 5 *B–D*). Compared with RNCs with shorter nascent chains, TF exerts an approximate twofold larger weakening effect on the binding of SRP to RNCs with longer nascent chains (Fig. 5 *B–D*). As a result, the affinity of SRP for RNC_{FtsQ} is weakened to 39 nM, that for RNC_{3A7L} is weakened to 53 nM, and that for RNC_{phoA} is weakened to 200 nM (Fig. 5 *B–D* and Table 1).

We next tested whether TF also prevents the targeting of long-chain RNCs to the membrane through SRP•FtsY assembly. With $RNC_{FtsQ\text{-}135}$, which contains a strongly hydrophobic TMD, SRP•FtsY complex assembly remains rapid at the longer chain length and is not significantly affected by TF (Fig. 5*E*). With RNC_{3A7L}, which contains a weaker signal sequence more representative of SRP-dependent secretory proteins, TF exerts a much larger inhibitory effect at the longer chain length, slowing the assembly of the targeting complex by 18-fold (Fig. 5*F* and Table 2). Analogous results were observed with $RNC_{phoA\text{-}130}$ (Fig. 5*G*). Thus, TF exerts a larger inhibitory effect on the membrane targeting of RNCs as the nascent chain elongates, and this effect occurs for both SRP-dependent and SRP-independent secretory protein substrates.

To evaluate the contribution of TF versus the intrinsic changes in SRP activity to the rejection of long-chain RNCs, we performed a numerical simulation using the thermodynamic and kinetic parameters obtained in Figs. 1, 4, and 5. First, we computed the fractional occupancy of SRP on RNCs (Fig. S5*A*). Second, an apparent rate constant was determined using the closed complex assembly rate constants and the estimated range of cellular FtsY concentration (Fig. S5 *B* and *D*) (59). Using these parameters, we calculated the amount of time required for SRP and FtsY to successfully deliver either short- (80mer) or long-chain (130mer) RNC_{3A7L} and RNC_{phoA} to the membrane in the presence or absence of TF (Fig. S5 *C* and *E*). With $RNC_{3A7L\text{-}80}$, targeting can be completed within 2 s. When the 3A7L nascent chain is lengthened to 130 residues, the amount of time needed to target $RNC_{3A7L\text{-}130}$ is lengthened, but only to ≥4 s in the absence of TF (Fig. S5 *C* and *E*, light pink). However, in the presence of TF, this value increases to 17–80 s, well beyond the time for the nascent protein to complete its synthesis on the ribosome (Fig. S5 *C* and *E*, dark pink and dashed line). Analogous observations were made with phoA: In the absence of TF, the intrinsic reductions in SRP activity at the longer nascent chain length would still allow $RNC_{phoA\text{-}130}$ to be targeted within a reasonable time window (Fig. S5 *C* and *E*, light pink). However, with TF present, SRP and FtsY require ≥53 s to target $RNC_{phoA\text{-}130}$ (Fig. S5 *C* and *E*, dark pink). Thus, with the help of TF, long-chain RNCs exit the cotranslational targeting pathway effectively.

Collectively, the results in this section show that at longer nascent chain lengths, TF more strongly inhibits SRP functions including binding of the RNC and recruitment of SRP receptor. These allosteric inhibitions from TF could contribute significantly to the rejection of RNC from the SRP pathway once the nascent chain reaches a critical length. This effect is observed with both SRP-dependent and SRP-independent secretory proteins but, surprisingly, is not pronounced with integral membrane protein substrates such as FtsQ.

TF Enhances the Specificity of SRP-Dependent Protein Targeting. Our results strongly suggest that TF will enhance the discrimination of SRP against borderline substrates, such as EspP and phoA. To test this hypothesis, we determined the effect of TF on the targeting efficiency of proteins with different signal sequences. We used a well-established heterologous assay in which various signal sequences are fused to the mature region of an established SRP substrate, preprolactin (pPL). The pPL variants are translated in a wheat germ extract (60, 61). The ability of *Escherichia coli* SRP and FtsY to mediate the cotranslational targeting of pPL variants to microsomal membranes is tested using cleavage of signal sequence to report on successful targeting and translocation (Fig. 6). Multiple factors render this assay an optimal choice for testing insights from biophysical studies of SRP in a complete targeting reaction: (*i*) Bacterial SRP and FtsY mediate pPL targeting as efficiently as their mammalian homologs despite the heterologous nature of this assay (61), highlighting the remarkable conservation of the SRP pathway; (*ii*) wheat germ extract is devoid of endogenous SRP and potential SRP regulators that may serve redundant functions as TF, which allows the effect of TF to be most readily unmasked; (*iii*) the microsomal membrane has much higher

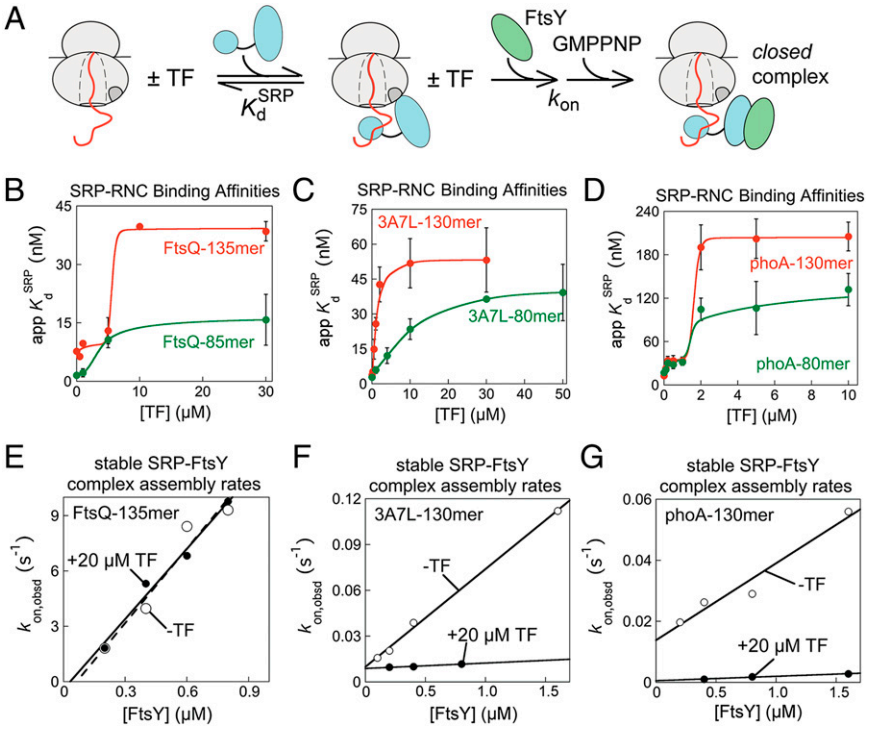

Fig. 5. TF more effectively inhibits SRP function at a longer nascent chain length. (*A*) Scheme depicting the two steps: binding of SRP to RNC and assembly of the closed targeting complex. (*B–D*) Effects of TF on the apparent binding affinity of SRP to RNC_{FtsQ} (*B*), RNC_{3A7L} (*C*), and RNC_{phoA} (*D*) when the nascent chain is 80–85 residues long (green lines) or 130–135 residues long (red lines). Error bars are SDs from two to three measurements or error estimates from fit of data, whichever is greater. (*E–G*) Effects of 20 μM TF on the assembly kinetics of the closed targeting complex with RNC_{FtsQ} (*E*), RNC_{3A7L} (*F*), and RNC_{phoA} (*G*) when the nascent chains are 130–135 residues long. Representative rate measurements are shown. The rate and equilibrium constants derived from two to three measurements are summarized in Tables 1 and 2.

cotranslational translocation activity than bacterial membrane vesicles (62–64), so that the output of the assay is not limited by the downstream translocation steps; and (*iv*) rapid cleavage of signal sequences by signal peptidase allows both the premature and mature proteins to be quantified, providing the most accurate quantification of targeting efficiency; analogous readouts are not available with bacterial membrane vesicles. Finally, the Sec translocon has a more relaxed specificity than SRP and translocates both cotranslational and posttranslationally targeted substrates (65); thus, the overall assay reports on the more stringent substrate selection by the SRP pathway.

In agreement with previous observations, 2A8L-pPL and 3A7L-pPL are efficiently targeted and translocated in this assay (Fig. 6 *A*, *B*, and *E*), whereas borderline substrates such as EspP and phoA retained ∼20–25% targeting (Fig. 6 *C–E*). Importantly, the presence of TF reduced the targeting of EspP-pPL and phoA-pPL to ∼5–10% but has negligible effects on the targeting and translocation of 2A8L-pPL and 3A7L-pPL (Fig. 6 *A–D*; summarized in Fig. 6*E*). This provides direct evidence that the complex interplay between SRP and TF contributes to enhancing the specificity of cotranslational protein targeting.

A mathematical model has been established that calculates the fraction of substrates that can be targeted by the SRP pathway based on the kinetic and thermodynamic parameters of three stages of the targeting cycle: cargo binding, SRP•FtsY assembly, and kinetic proofreading using GTP hydrolysis (Fig. S1) (40). Using this model and the rate and equilibrium constants determined here, we numerically simulated how TF affects the fraction of substrates retained at each step of the SRP pathway. The calculation shows that TF exerts a very modest effect on the fraction of RNC bound by SRP: Although SRP occupies >95% of all four RNCs in the absence of TF (Fig. 7*A*, light gray bars), TF brings the occupancy of SRP on RNC_{FtsQ}, RNC_{3A7L}, and RNC_{EspP} to ∼90%, and that of RNC_{phoA} to 75% (Fig. 7*B*, light gray bars). In the membrane targeting step, >90% of RNC_{FtsQ} and RNC_{3A7L} are retained in the SRP pathway (Fig. 7*A*) with or without TF. Without TF, ∼96% and 59% of RNC_{phoA} and RNC_{EspP} remain in the SRP pathway despite being SRP-independent substrates (Fig. 7*A*, dark gray bars) whereas, with TF present, the amount of RNC_{phoA} and RNC_{EspP} that remains in the SRP pathway is lowered to 42% and 9.2%, respectively, after the targeting step (Fig. 7*B*, dark gray bars). Additional substrates were rejected through competition between GTP hydrolysis and cargo unloading (dark bars) (40). The overall targeting efficiencies predicted by the numerical analysis agreed well with the results of the targeting and translocation assays in both the presence and absence of TF (Fig. 7 *C* and *D*), suggesting that this model reasonably captures the molecular determinants that govern the selectivity of the SRP pathway.

Discussion

Numerous factors, including molecular chaperones, modification enzymes, quality control complexes, and protein targeting

Table 1. Summary of the effect of nascent chain length on SRP–RNC binding affinities

	K_d^{SRP}, nM		
RNC	80mer	130mer	130mer, +TF
FtsQ	1.5 ± 0.6	7.7 ± 0.4	39.1 ± 0.8
3A7L	2.8 ± 0.9	3.9 ± 0.8	52.5 ± 1.0
phoA	17.2 ± 3.0	12.7 ± 2.9	199 ± 8

Error bars are SDs from two to three experiments.

Table 2. Summary of the effect of nascent chain length on SRP•FtsY closed complex assembly rates

RNC	k_{on}^{FtsY}, 10^6 $M^{-1}\cdot s^{-1}$		
	80mer	130mer	130mer, +TF
FtsQ	18.5 ± 0.90	12.7 ± 1.3	13.5 ± 2.3
3A7L	0.145 ± 0.04	0.064 ± 0.024	0.0035 ± 0.0006
phoA	0.0635 ± 0.01	0.025 ± 0.0039	0.0014 ± 0.0002

Error bars are SDs from two to three experiments.

machineries, bind to the ribosome near the exit site and direct nascent polypeptides to distinct biogenesis pathways. Accurate selection of the nascent protein into the correct biogenesis pathway is essential to maintain the homeostasis of the proteome. In recent years, there has been an increasing number of structures of individual protein biogenesis factors bound to the ribosome exit site (3, 18, 26, 56, 66–74), as well as efforts to globally catalog the nascent polypeptides they occupy (9, 13). However, the key question remains: Given the crowded environment at the ribosome exit site and a limited time window of action, how does a nascent polypeptide engage the correct set of factors and hence commit to its correct biogenesis pathway? Using SRP and TF as a model system, this work reveals a multitude of molecular mechanisms by which TF and SRP regulate each other's function. This interplay allows SRP to better discriminate against borderline cargos and thus ensures the correct partitioning of proteins to their respective biogenesis pathways.

TF regulates SRP at three distinct stages (Fig. 7*E*). As the nascent polypeptide begins to emerge from the ribosome exit site (≤85 amino acids), TF weakens the SRP–RNC interaction by up to an order of magnitude (step 1). A mathematical analysis shows that this modulation translates into a modest change in the occupancy of SRP on the translating ribosomes, allowing TF to help remove a small fraction (~20%) of SRPs from RNCs bearing some of the Sec-dependent substrates, such as phoA, at an early stage (Fig. 7*E*, step 1). In the second stage, TF selectively reduces the rates for stable SRP•FtsY complex assembly for RNCs bearing SecA/B-dependent, but not SRP-dependent, substrates (Fig. 7*E*, step 2), and thus slows the delivery of these RNCs to the target membrane. The kinetics of SRP•FtsY assembly is a crucial checkpoint in cotranslational protein targeting (34, 40). Here, we find that TF further enhances the kinetic discrimination of SRP against suboptimal substrates during this step (Fig. 4*F*), significantly reducing the amount of RNC_{phoA} and RNC_{EspP} that remains in the SRP pathway after membrane targeting (Fig. S5*B*, dark gray bars).

In the third regulatory event, TF helps reject substrates from SRP when the nascent chain is elongated beyond a critical length (Fig. 7*E*, step 3). Rejection of long-chain RNCs is critical for maintaining the selectivity of SRP, as it sets a "timer" that irreversibly removes substrates that fail to complete targeting within a given time window. Indeed, slower translation elongation, which gives SRP a longer time window, allows substrates with weaker signal sequences to enter the SRP pathway (75). The results of this and previous work (47, 57, 58) show that multiple mechanisms together impose this timer. First, RNC–SRP binding affinity could weaken modestly with long-chain RNCs. Second, recruitment of FtsY to RNC•SRP complexes slows twofold to threefold when the nascent chain becomes longer. Importantly, TF exerts a larger inhibitory effect on both of these steps at the longer nascent chain length, and thus aids in the rejection of long-chain RNCs from the SRP pathway (Fig. S5). Finally, we found that even this timer is set differentially: Targeting of SRP substrates containing integral TMDs was less sensitive to the nascent chain length, whereas secretory proteins with strong and weak signal sequences are strongly discriminated.

As would be predicted from these biophysical properties, TF enhances the selectivity of SRP and helps prevent suboptimal substrates, such as phoA and EspP, from leaking into the SRP pathway (Fig. 7 *A–D*). This could help prioritize limited amounts of SRP in a cell for strictly cotranslational substrates. The results of the targeting and translocation reactions, both in the presence and absence of TF, agree well with predictions from a mathematical analysis based on the kinetic and thermodynamic parameters for different stages of the targeting cycle (Fig. 6 and Fig. S1) (40). This analysis highlights the importance of kinetic control at the SRP•FtsY assembly step as a major checkpoint that discriminates against suboptimal substrates. It also shows that TF allows suboptimal substrates to be rejected at an earlier stage (membrane targeting) and reduces the fraction of substrates that reaches the membrane and has to be rejected by proofreading (Fig. 7 *A–D*).

Reciprocally, SRP helps TF engage the correct substrates. At early stages, TF binds with comparable affinities to RNCs bearing nascent chains belonging to both the cotranslational and posttranslational targeting pathways, and even exhibits twofold

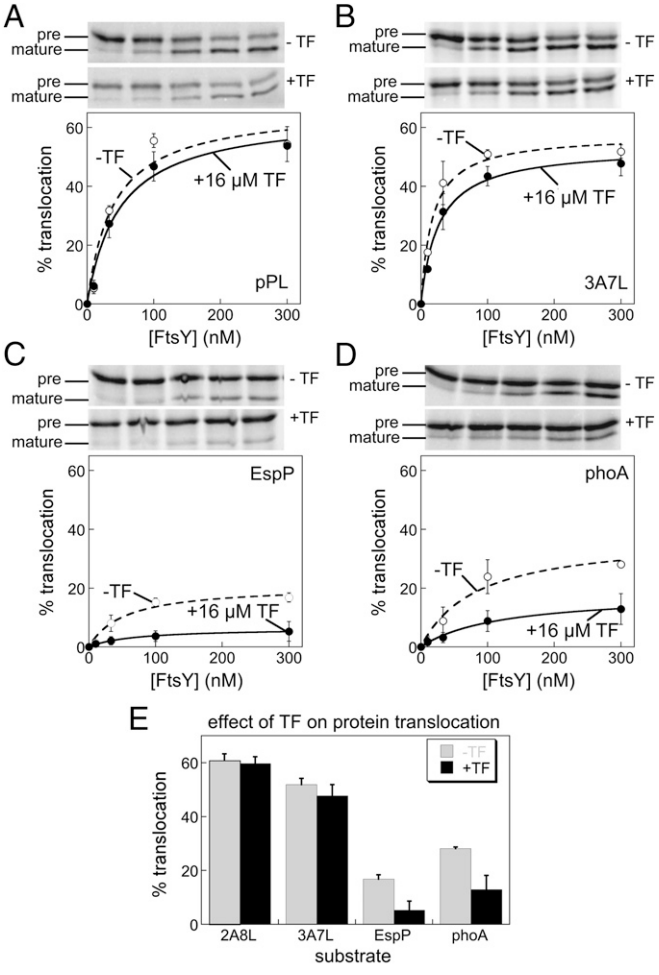

Fig. 6. TF enhances the specificity of SRP-dependent targeting to ER membrane. (*A–D*) Translocation of 2A8L-pPL (*A*), 3A7L-pPL (*B*), EspP-pPL (*C*), and phoA-pPL (*D*) by SRP and FtsY (0 nM, 10 nM, 33 nM, 100 nM, and 300 nM) in the absence (○) or presence (●) of 16 μM TF. In each panel, representative gels are shown (*Top*) with quantification of the gel (*Bottom*). (*E*) Summary of translocation efficiencies at saturating FtsY concentrations with and without TF. Error bars are SDs from three to four independent experiments.

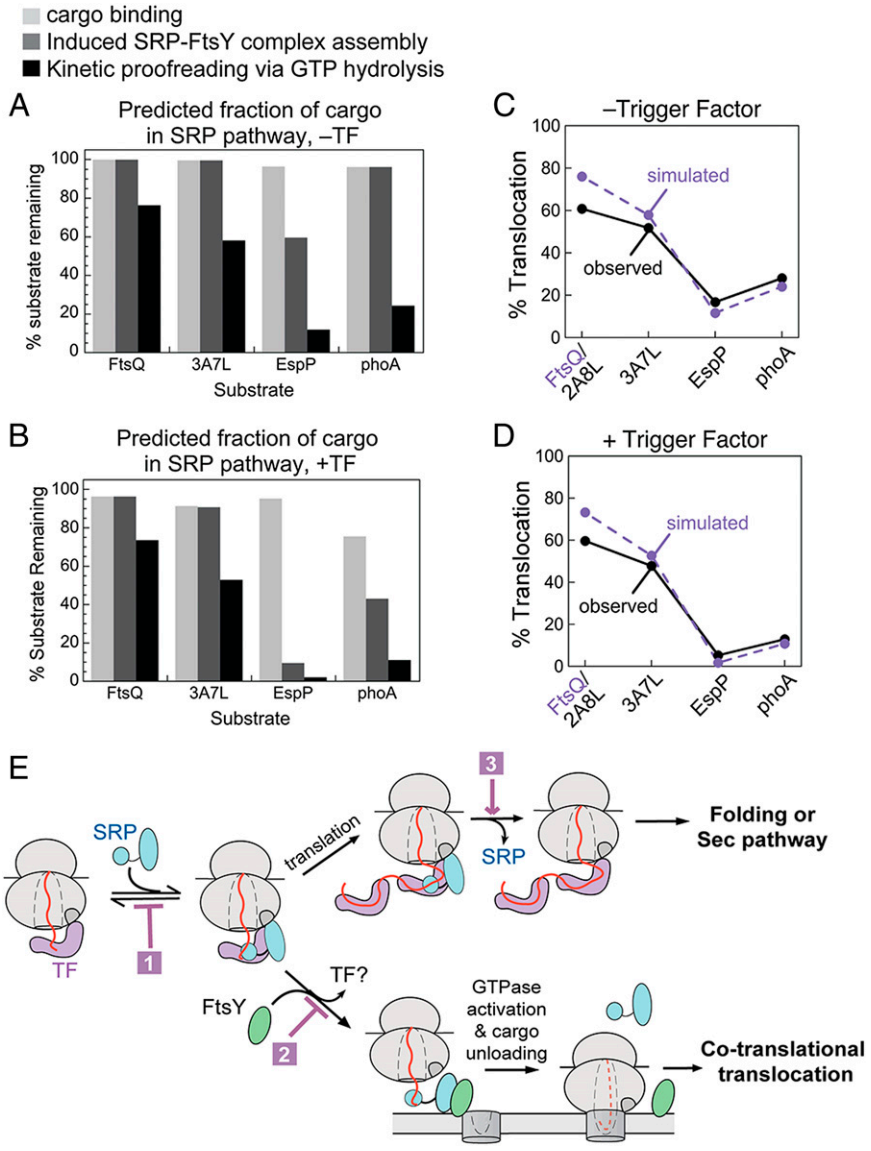

Fig. 7. Mathematical simulations and model describing the molecular mechanism of substrate partitioning into the SRP or TF pathway. (*A* and *B*) Mathematical simulations of the fraction of substrates that remain in the SRP pathway at different stages without (*A*) and with (*B*) TF. Light gray bars denote the fraction of RNC retained at the SRP binding step; dark gray bars denote the fraction of RNC retained after assembly of the closed SRP•FtsY complex; black bars denote the fraction of RNC remaining in the pathway after kinetic proofreading via GTP hydrolysis. (*C* and *D*) Comparison of predicted (dashed) and experimentally determined (solid) efficiencies of targeting and translocation of the model substrates by the SRP targeting pathway without (*C*) and with (*D*) TF. The values plotted are obtained from Fig. 6*E* (black bars) and Fig. 7 *A* and *B*. (*E*) TF regulates SRP at three steps: (*i*) SRP binding to RNC, (*ii*) targeting of RNC to the membrane via SRP•FtsY assembly, and (*iii*) removal of SRP from ribosomes when the nascent polypeptide exceeds a critical length.

to fourfold higher affinity for RNCs bearing FtsQ and 3A7L than the phoA and EspP substrates (Fig. 2*E* and ref. 20). This is not surprising given the preference of TF for hydrophobic sequences (4, 45). It is via the regulation by SRP and FtsY, rather than the intrinsic affinity of TF for RNCs, that substrates such as FtsQ and 3A7L are removed from TF, allowing it to select and commit to Sec-dependent substrates.

Collectively, the results here demonstrate a multilayered mechanism for the selection of nascent proteins into distinct biogenesis pathways (Fig. 7*E*). Given the high cellular concentration of TF, it is bound to >98% of translating ribosomes. There, TF alters the affinity and conformation of SRP binding to nascent polypeptides that emerge from the ribosome (step 1). This effect is modest, and removes a small fraction of SRP from some ribosomes bearing SRP-independent substrates. The majority of RNCs accumulate as ternary complexes with SRP and TF. For RNCs bearing SRP-dependent substrates, delivery to the membrane via FtsY recruitment is rapid and unaffected by TF; these substrates are hence selected into the cotranslational targeting and translocation pathway (Fig. 7*E*). In contrast, for RNCs bearing SRP-independent substrates, membrane targeting is slow and further slowed by TF (step 2). While these RNC•SRP•TF complexes bide for membrane targeting, ongoing protein synthesis quickly elongates the nascent polypeptide beyond a critical length, at which TF more effectively inhibits SRP functions (step 3). These proteins are hence rejected from SRP and sorted to either cytoplasmic folding or the posttranslational SecA/B pathway (Fig. 7*E*).

Our model reconciles many previous observations. The model that SRP and TF accumulate as ternary complexes with RNCs is consistent with cosedimentation, crosslinking, and FRET analyses (17, 19, 20). The ability of TF to alter the interaction of SRP

with signal sequences is also consistent with less efficient cross-links of SRP to nascent chains in the presence of TF (15). These data also show that, in the presence of other RNC-interacting factors, the initial interaction of TF/SRP with RNCs is more dynamic at short nascent chain lengths and that commitment of nascent proteins to TF occurs at longer nascent chain lengths. This explains the observation in ribosome-profiling experiments, where TF was found to stably associate with RNCs bearing SRP-independent substrates at nascent chain lengths >100 residues (13).

Our results emphasize the crowded environment at the ribosome exit site. The effect of TF in weakening RNC–SRP binding does not follow a hyperbolic concentration dependence expected for binding of a single TF molecule to each RNC, but rather displays a complex pattern (Fig. 5 *B–D*) indicative of the binding of multiple TFs to the RNC (Fig. 7*E*) as proposed previously (45). Further, the observation that TF alters the FRET value of SRP•FtsY early complexes strongly suggests that all three factors are present on the RNC at this stage. Our findings also suggest a remarkable degree of structural plasticity for cotranslational biogenesis machineries bound at the ribosome exit site, wherein each factor could alter its conformation to accommodate another factor bound in the vicinity. In support of this model, multiple conformations of SRP bound to RNCs have been observed recently in fluorescence and single-molecule studies (34, 58). Regulation of SRP conformation by TF presumably leads to the observed weaker binding to RNCs and the slower recruitment of FtsY in the membrane-targeting step. How the ribosome exit site accommodates multiple factors, how SRP and the SRP•FtsY complex transition between alternative conformations in response to the signal sequence, and how this conformational flexibility is exploited by TF to enhance selectivity remain intriguing questions for future investigations.

Accurate selection of nascent proteins into distinct fates is at the heart of proper protein biogenesis. In additional to TF, additional factors that interact with the RNC could exert analogous regulations on SRP, TF, or other protein biogenesis machineries. The results here provide an example for how this regulation can help enhance the fidelity of substrate selection, and a conceptual framework for considering how nascent proteins are accurately sorted among other biogenesis machineries at the ribosome exit site, or in other crowded cellular environments.

Methods

Materials. The *E. coli* Ffh, FtsY, 4.5S RNA, and TF were expressed and purified using established protocols (76, 77). Single cysteine mutations were introduced via Quikchange mutagenesis (Stratagene). Mutant proteins were purified using the same procedures as wild-type protein. Ffh (C153) was labeled with DACM and FtsY (C345), Ffh (C421), and TF (C377) were labeled with BODIPY-FL-*N*-(2-aminoethyl)-maleimide (Invitrogen) as described previously (32). Labeled proteins were purified from unconjugated dye using gel filtration chromatography on Sephadex G-25 resin (Sigma) as described (32). Labeling efficiencies were usually >90%. Homogenous RNCs were generated by in vitro translation and stalled using the sequence SEKGYRIDYAHFTPQAKFSTPVWISQAQGIRAGPQRLS from the *E. coli* SecM protein (78). Translation stalling occurs at the underlined G, and the C-terminal PQRLS residues are not incorporated into the nascent chain. Short-chain and long-chain RNCs contain 80–85 and 130–135 amino acids, respectively, between the N terminus of signal sequence and the peptidyl transferase center of ribosome. RNCs were affinity-purified via the strep$_3$ tag on the nascent polypeptide, as described (41, 48, 78). The quality of RNC was documented in ref. 78. RNCs purified through this procedure are identical in their ability to bind SRP and accelerate SRP•FtsY assembly as RNCs further purified by sucrose gradient centrifugation (33, 40). Amber suppression technology to incorporate Cm into the nascent polypeptide is described in detail in ref. 48.

Fluorescence Measurements. All fluorescence measurements were carried out on a FluoroLog-3-22 spectrofluorometer (Jobin-Yvon) or an SF-2004 stopped-flow apparatus (KinTek) in assay buffer [50 mM KHEPES pH 7.5, 150 mM KOAc, 10 mM Mg(OAc)$_2$ and 2 mM DTT] at 25 °C. Details of the design and analysis of experiments are found in *SI Methods*.

Cotranslational Protein Targeting and Translocation Assay. The protein targeting efficiency of SRP, with or without TF, was determined by a cotranslational translocation assay using [^{35}S]methionine-labeled pPL as a substrate, as described previously (60). The signal sequences of 3A7L, EspP, and phoA were fused to the mature region of prolactin. Reactions were carried out using 345 nM SRP, 0 μM or 16 μM TF, varying concentrations of FtsY (specified in figure legends), and 1.5 equivalent of trypsin-digested EDTA and salt-washed ER microsomal membranes. Reactions were analyzed by SDS/PAGE followed by autoradiography. Mathematical modeling of targeting efficiency is described in *SI Methods*.

ACKNOWLEDGMENTS. We thank Xin Zhang and Kuang Shen for insightful discussions, and Harris Bernstein and members of the S.-o.S. group for comments on the manuscript. This work was supported by National Institutes of Health (NIH) Grant GM078024 to S.-o.S. and the NIH NIGMS Ruth L. Kirschstein National Research Service Award (F31GM095294) to A.A. This project was funded in part by the Henry Dreyfus Teacher-Scholar Award, the Packard and Lucile Fellowship in science and engineering, and the Gordon and Betty Moore Foundation through Grant GBMF2939 (to S.-o.S.).

1. Merz F, et al. (2008) Molecular mechanism and structure of Trigger Factor bound to the translating ribosome. *EMBO J* 27(11):1622–1632.
2. Fedyukina DV, Cavagnero S (2011) Protein folding at the exit tunnel. *Annu Rev Biophys* 40:337–359.
3. Ferbitz L, et al. (2004) Trigger factor in complex with the ribosome forms a molecular cradle for nascent proteins. *Nature* 431(7008):590–596.
4. Lakshmipathy SK, et al. (2007) Identification of nascent chain interaction sites on trigger factor. *J Biol Chem* 282(16):12186–12193.
5. Schlünzen F, et al. (2005) The binding mode of the trigger factor on the ribosome: Implications for protein folding and SRP interaction. *Structure* 13(11):1685–1694.
6. Lill R, Crooke E, Guthrie B, Wickner W (1988) The "trigger factor cycle" includes ribosomes, presecretory proteins, and the plasma membrane. *Cell* 54(7):1013–1018.
7. Deuerling E, Schulze-Specking A, Tomoyasu T, Mogk A, Bukau B (1999) Trigger factor and DnaK cooperate in folding of newly synthesized proteins. *Nature* 400(6745):693–696.
8. Beck K, Wu LF, Brunner J, Müller M (2000) Discrimination between SRP- and SecA/SecB-dependent substrates involves selective recognition of nascent chains by SRP and trigger factor. *EMBO J* 19(1):134–143.
9. del Alamo M, et al. (2011) Defining the specificity of cotranslationally acting chaperones by systematic analysis of mRNAs associated with ribosome-nascent chain complexes. *PLoS Biol* 9(7):e1001100.
10. Eisner G, Moser M, Schäfer U, Beck K, Müller M (2006) Alternate recruitment of signal recognition particle and trigger factor to the signal sequence of a growing nascent polypeptide. *J Biol Chem* 281(11):7172–7179.
11. Powers T, Walter P (1996) The nascent polypeptide-associated complex modulates interactions between the signal recognition particle and the ribosome. *Curr Biol* 6(3):331–338.
12. Lee HC, Bernstein HD (2002) Trigger factor retards protein export in *Escherichia coli*. *J Biol Chem* 277(45):43527–43535.
13. Oh E, et al. (2011) Selective ribosome profiling reveals the cotranslational chaperone action of trigger factor in vivo. *Cell* 147(6):1295–1308.
14. Kramer G, Boehringer D, Ban N, Bukau B (2009) The ribosome as a platform for co-translational processing, folding and targeting of newly synthesized proteins. *Nat Struct Mol Biol* 16(6):589–597.
15. Ullers RS, et al. (2006) Sequence-specific interactions of nascent *Escherichia coli* polypeptides with trigger factor and signal recognition particle. *J Biol Chem* 281(20):13999–14005.
16. Ullers RS, et al. (2003) Interplay of signal recognition particle and trigger factor at L23 near the nascent chain exit site on the *Escherichia coli* ribosome. *J Cell Biol* 161(4):679–684.
17. Buskiewicz I, et al. (2004) Trigger factor binds to ribosome-signal-recognition particle (SRP) complexes and is excluded by binding of the SRP receptor. *Proc Natl Acad Sci USA* 101(21):7902–7906.
18. Schaffitzel C, et al. (2006) Structure of the *E. coli* signal recognition particle bound to a translating ribosome. *Nature* 444(7118):503–506.
19. Raine A, Ivanova N, Wikberg JE, Ehrenberg M (2004) Simultaneous binding of trigger factor and signal recognition particle to the *E. coli* ribosome. *Biochimie* 86(7):495–500.
20. Bornemann T, Holtkamp W, Wintermeyer W (2014) Interplay between trigger factor and other protein biogenesis factors on the ribosome. *Nat Commun* 5:4180.
21. Huber D, et al. (2011) SecA interacts with ribosomes in order to facilitate post-translational translocation in bacteria. *Mol Cell* 41(3):343–353.
22. Beckmann R, et al. (2001) Architecture of the protein-conducting channel associated with the translating 80S ribosome. *Cell* 107(3):361–372.
23. Mitra K, et al. (2005) Structure of the *E. coli* protein-conducting channel bound to a translating ribosome. *Nature* 438(7066):318–324.
24. Houben ENG, et al. (2002) YidC and SecY mediate membrane insertion of a Type I transmembrane domain. *J Biol Chem* 277(39):35880–35886.

25. Wickles S, et al. (2014) A structural model of the active ribosome-bound membrane protein insertase YidC. *eLife* 3:e03035.
26. Brandman O, et al. (2012) A ribosome-bound quality control complex triggers degradation of nascent peptides and signals translation stress. *Cell* 151(5):1042–1054.
27. Bengtson MH, Joazeiro CA (2010) Role of a ribosome-associated E3 ubiquitin ligase in protein quality control. *Nature* 467(7314):470–473.
28. Defenouillère Q, et al. (2013) Cdc48-associated complex bound to 60S particles is required for the clearance of aberrant translation products. *Proc Natl Acad Sci USA* 110(13):5046–5051.
29. Inada T (2013) Quality control systems for aberrant mRNAs induced by aberrant translation elongation and termination. *Biochim Biophys Acta* 1829(6-7):634–642.
30. Verma R, Oania RS, Kolawa NJ, Deshaies RJ (2013) Cdc48/p97 promotes degradation of aberrant nascent polypeptides bound to the ribosome. *eLife* 2:e00308.
31. Akopian D, Shen K, Zhang X, Shan S-O (2013) Signal recognition particle: An essential protein-targeting machine. *Annu Rev Biochem* 82:693–721.
32. Zhang X, Kung S, Shan SO (2008) Demonstration of a multistep mechanism for assembly of the SRP x SRP receptor complex: Implications for the catalytic role of SRP RNA. *J Mol Biol* 381(3):581–593.
33. Zhang X, Schaffitzel C, Ban N, Shan SO (2009) Multiple conformational switches in a GTPase complex control co-translational protein targeting. *Proc Natl Acad Sci USA* 106(6):1754–1759.
34. Holtkamp W, et al. (2012) Dynamic switch of the signal recognition particle from scanning to targeting. *Nat Struct Mol Biol* 19(12):1332–1337.
35. Zhang X, et al. (2011) Direct visualization reveals dynamics of a transient intermediate during protein assembly. *Proc Natl Acad Sci USA* 108(16):6450–6455.
36. Egea PF, et al. (2004) Substrate twinning activates the signal recognition particle and its receptor. *Nature* 427(6971):215–221.
37. Focia PJ, Shepotinovskaya IV, Seidler JA, Freymann DM (2004) Heterodimeric GTPase core of the SRP targeting complex. *Science* 303(5656):373–377.
38. Lam VQ, Akopian D, Rome M, Henningsen D, Shan S-O (2010) Lipid activation of the signal recognition particle receptor provides spatial coordination of protein targeting. *J Cell Biol* 190(4):623–635.
39. Zhang X, Shan S-O (2014) Fidelity of cotranslational protein targeting by the signal recognition particle. *Annu Rev Biophys* 43:381–408.
40. Zhang X, Rashid R, Wang K, Shan SO (2010) Sequential checkpoints govern substrate selection during cotranslational protein targeting. *Science* 328(5979):757–760.
41. Saraogi I, Akopian D, Shan S-O (2014) Regulation of cargo recognition, commitment, and unloading drives cotranslational protein targeting. *J Cell Biol* 205(5):693–706.
42. Shen K, Zhang X, Shan S-O (2011) Synergistic actions between the SRP RNA and translating ribosome allow efficient delivery of the correct cargos during cotranslational protein targeting. *RNA* 17(5):892–902.
43. Maier R, Eckert B, Scholz C, Lilie H, Schmid FX (2003) Interaction of trigger factor with the ribosome. *J Mol Biol* 326(2):585–592.
44. Kramer G, et al. (2002) L23 protein functions as a chaperone docking site on the ribosome. *Nature* 419(6903):171–174.
45. Kaiser CM, et al. (2006) Real-time observation of trigger factor function on translating ribosomes. *Nature* 444(7118):455–460.
46. Rutkowska A, et al. (2008) Dynamics of trigger factor interaction with translating ribosomes. *J Biol Chem* 283(7):4124–4132.
47. Siegel V, Walter P (1988) The affinity of signal recognition particle for presecretory proteins is dependent on nascent chain length. *EMBO J* 7(6):1769–1775.
48. Saraogi I, Zhang D, Chandrasekaran S, Shan S-O (2011) Site-specific fluorescent labeling of nascent proteins on the translating ribosome. *J Am Chem Soc* 133(38): 14936–14939.
49. Valent QA, et al. (1995) Early events in preprotein recognition in *E. coli*: Interaction of SRP and trigger factor with nascent polypeptides. *EMBO J* 14(22):5494–5505.
50. von Loeffelholz O, et al. (2013) Structural basis of signal sequence surveillance and selection by the SRP-FtsY complex. *Nat Struct Mol Biol* 20(5):604–610.
51. Szabady RL, Peterson JH, Skillman KM, Bernstein HD (2005) An unusual signal peptide facilitates late steps in the biogenesis of a bacterial autotransporter. *Proc Natl Acad Sci USA* 102(1):221–226.
52. Peterson JH, Szabady RL, Bernstein HD (2006) An unusual signal peptide extension inhibits the binding of bacterial presecretory proteins to the signal recognition particle, trigger factor, and the SecYEG complex. *J Biol Chem* 281(14):9038–9048.
53. Valent QA, et al. (1997) Nascent membrane and presecretory proteins synthesized in *Escherichia coli* associate with signal recognition particle and trigger factor. *Mol Microbiol* 25(1):53–64.
54. Walter P, Blobel G (1981) Translocation of proteins across the endoplasmic reticulum III. Signal recognition protein (SRP) causes signal sequence-dependent and site-specific arrest of chain elongation that is released by microsomal membranes. *J Cell Biol* 91(2 Pt 1):557–561.
55. Saraogi I, Shan SO (2011) Molecular mechanism of co-translational protein targeting by the signal recognition particle. *Traffic* 12(5):535–542.
56. Estrozi LF, Boehringer D, Shan S-O, Ban N, Schaffitzel C (2011) Cryo-EM structure of the *E. coli* translating ribosome in complex with SRP and its receptor. *Nat Struct Mol Biol* 18(1):88–90.
57. Flanagan JJ, et al. (2003) Signal recognition particle binds to ribosome-bound signal sequences with fluorescence-detected subnanomolar affinity that does not diminish as the nascent chain lengthens. *J Biol Chem* 278(20):18628–18637.
58. Noriega TR, et al. (2014) Signal recognition particle-ribosome binding is sensitive to nascent chain length. *J Biol Chem* 289(28):19294–19305.
59. Drew D, Fröderberg L, Baars L, de Gier J-WL (2003) Assembly and overexpression of membrane proteins in *Escherichia coli*. *Biochim Biophys Acta* 1610(1):3–10.
60. Shan S-O, Chandrasekar S, Walter P (2007) Conformational changes in the GTPase modules of the signal reception particle and its receptor drive initiation of protein translocation. *J Cell Biol* 178(4):611–620.
61. Powers T, Walter P (1997) Co-translational protein targeting catalyzed by the *Escherichia coli* signal recognition particle and its receptor. *EMBO J* 16(16):4880–4886.
62. Schulze RJ, et al. (2014) Membrane protein insertion and proton-motive-force-dependent secretion through the bacterial holo-translocon SecYEG-SecDF-YajC-YidC. *Proc Natl Acad Sci USA* 111(13):4844–4849.
63. Koch HG, et al. (1999) In vitro studies with purified components reveal signal recognition particle (SRP) and SecA/SecB as constituents of two independent protein-targeting pathways of *Escherichia coli*. *Mol Biol Cell* 10(7):2163–2173.
64. Neumann-Haefelin C, Schäfer U, Müller M, Koch HG (2000) SRP-dependent co-translational targeting and SecA-dependent translocation analyzed as individual steps in the export of a bacterial protein. *EMBO J* 19(23):6419–6426.
65. Valent QA, et al. (1998) The *Escherichia coli* SRP and SecB targeting pathways converge at the translocon. *EMBO J* 17(9):2504–2512.
66. Leidig C, et al. (2013) Structural characterization of a eukaryotic chaperone—The ribosome-associated complex. *Nat Struct Mol Biol* 20(1):23–28.
67. Frauenfeld J, et al. (2011) Cryo-EM structure of the ribosome-SecYE complex in the membrane environment. *Nat Struct Mol Biol* 18(5):614–621.
68. Gogala M, et al. (2014) Structures of the Sec61 complex engaged in nascent peptide translocation or membrane insertion. *Nature* 506(7486):107–110.
69. Knoops K, Schoehn G, Schaffitzel C (2012) Cryo-electron microscopy of ribosomal complexes in cotranslational folding, targeting, and translocation. *Wiley Interdiscip Rev RNA* 3(3):429–441.
70. Bingel-Erlenmeyer R, et al. (2008) A peptide deformylase-ribosome complex reveals mechanism of nascent chain processing. *Nature* 452(7183):108–111.
71. Kohler R, et al. (2009) YidC and Oxa1 form dimeric insertion pores on the translating ribosome. *Mol Cell* 34(3):344–353.
72. Halic M, et al. (2006) Following the signal sequence from ribosomal tunnel exit to signal recognition particle. *Nature* 444(7118):507–511.
73. Park E, et al. (2014) Structure of the SecY channel during initiation of protein translocation. *Nature* 506(7486):102–106.
74. Voorhees RM, Fernández IS, Scheres SH, Hegde RS (2014) Structure of the mammalian ribosome-Sec61 complex to 3.4 Å resolution. *Cell* 157(7):1632–1643.
75. Zhang D, Shan S-O (2012) Translation elongation regulates substrate selection by the signal recognition particle. *J Biol Chem* 287(10):7652–7660.
76. Peluso P, Shan SO, Nock S, Herschlag D, Walter P (2001) Role of SRP RNA in the GTPase cycles of Ffh and FtsY. *Biochemistry* 40(50):15224–15233.
77. Kramer G, et al. (2004) Functional dissection of *Escherichia coli* trigger factor: Unraveling the function of individual domains. *J Bacteriol* 186(12):3777–3784.
78. Schaffitzel C, Ban N, Shan S-O (2007) Generation of ribosome nascent chain complexes for structural and functional studies. *J Struct Biol* 158(3):463–471.